Estimation of winter wheat LAI and SPAD based on the fusion of texture features and vegetation indices from UAV images

Xingjiao Yu[1,2], Xuefei Huo[1,2], Long Qian[1,2], Yingying Pi[1,2], Yafei Wang[1,2], Kai Fan[1,2], Qi Yin[1,2], Xiaotao Hu[1,2], Wen'e Wang[1,2*]

(1. *Key Laboratory of Agricultural Soil and Water Engineering in Arid and Semiarid Areas, Ministry of Education, Northwest A&F University, Yangling 712100, Shaanxi, China*;
2. *College of Water Resources and Architectural Engineering, Northwest A&F University, Yangling 712100, Shaanxi, China*)

Abstract: Accurate and efficient quantitative estimation of leaf area index (LAI) and soil and plant analyzer development (SPAD) in winter wheat is significant for field management decisions and yield prediction. This study compared the performance of three linear regression techniques: multiple linear regression (MLR), ridge regression (RR), and partial least squares regression (PLSR) and three machine learning algorithms: back-propagation neural networks (BP), random forests (RF), and support vector machine (SVM) with spectral vegetation indices (VIs), texture features (TEs), and their combinations extracted from UAV RGB images. A total of 36 estimation models were constructed, which included 24 models based on single datasets (VIs-based and TEs-based), and 12 models based on data fusion (VIs+TEs-based). The results revealed that combining VIs and TEs improved the accuracy of LAI and SPAD estimation for wheat compared to using VIs or TEs alone. Moreover, different data dimensionality reduction methods, including principal component analysis (PCA) and stepwise selection (ST), were used to improve the accuracy of LAI and SPAD estimation. The results showed that ST, PCA, and ST_PCA methods have different impacts on the accuracy of estimating crop parameters with the combination of VIs and TEs, where ST_PCA is effective in dealing with high-dimensional data and maintaining the accuracy of the model. The RF model combined with ST_PCA for integrating VIs and TEs achieved the best estimations, with R^2 of 0.86 and 0.91, RMSE of 0.26 and 2.01, and MAE of 0.22 and 1.66 for LAI and SPAD, respectively. ST_PCA, combined with machine learning algorithms, holds promising potential for monitoring crop physiological and biochemical parameters.

Keywords: LAI, SPAD, texture features, vegetation indices, stepwise selection, PCA
DOI: 10.25165/j.ijabe.20261904.8969

Citation: Yu X J, Huo X F, Qian L, Pi Y Y, Wang Y F, Fan K, et al. Estimation of winter wheat LAI and SPAD based on the fusion of texture features and vegetation indices from UAV images. Int J Agric & Biol Eng, 2026; 19(4): 292–306.

1 Introduction

Winter wheat, as one of the world's three major grain crops, constitutes the staple diet for over 35% of the global population[1-3]. Accurate and efficient quantitative estimation of wheat's physical and chemical parameters is of significant importance for yield prediction and field management. Among these parameters, leaf area index (LAI) and soil and plant analyzer development (SPAD) are key variables for photosynthesis, respiration, and transpiration in crops. They closely correlate with the capacity for photosynthetically active radiation and function as crucial indicators for the growth stages of crops and various stresses, whether biotic or abiotic[4,5]. Measurement of LAI and SPAD contributes to monitoring the physiological health of crops, detecting growth stress, and estimating yield[6-8]. However, traditional methods for obtaining LAI and SPAD rely on extensive field sampling and indoor experiments, which are not only time-consuming and labor-intensive but also invasive and delayed.

UAV remote sensing has rapidly evolved into a crucial tool for agricultural monitoring, driven by its advantages of low cost, high flexibility, and the ability to acquire high temporal and spatial resolution data on demand[9-12]. Various remote sensing data, including hyperspectral, multispectral, and thermal infrared, are widely used for estimating crop parameters such as leaf area index[13-15], soil and plant analyzer development[16-18], above-ground biomass[19-21], and so on. Research in this domain can generally be classified into two major categories: 1) models based on physical principles[8,22] and 2) models based on empirical regression[23,24]. Physical models exhibit high robustness but necessitate multiple parameter inputs, which poses a challenge. This significantly limits the practical application of physical models[25,26]. Conversely, empirical models utilize the physiological and biochemical parameters of crops together with vegetation indices to establish relationships that aim to highlight crop characteristics and are widely employed for crop monitoring[27-29]. Since the 1970s, Rouse et

Received date: 2024-03-29 **Accepted date:** 2025-08-24

Biographies: Xingjiao Yu, PhD candidate, research interest: all-weather monitoring of soil and crops based on multi-source remote sensing synergy, Email: yxj0204@nwafu.edu.com; **Xuefei Huo**, PhD candidate, research interest: crop water and nitrogen diagnostics using satellite remote sensing, Email: hxf@nwafu.edu.cn; **Long Qian**, PhD candidate, research interest: agricultural remote sensing and efficient utilization of water resources, Email: qianlong9611@126.com; **Yingying Pi**, MS, research interest: optimization and regulation of water resources; Email: ddp258013@163.com; **Yafei Wang**, MS, Email: wangyafei2022@nwafu.edu.cn; **Kai Fan**, MS, research interest: optimization and regulation of water resources, Email: 2022050889@nwafu.edu.cn; **Qi Yin**, MS candidatet, research interest: optimization and regulation of water resources, Email: yq2023055852@nwafu.edu.cn; **Xiaotao Hu**, PhD, research interest: remote sensing-based diagnosis of crop water stress, Email: huxiaotao11@nwsuaf.edu.cn.

***Corresponding author: Wen'e Wang**, Professor, research interest: theory and technology of water-saving irrigation. Key Laboratory of Agricultural Soil and Water Engineering in Arid and Semiarid Areas, Ministry of Education, Northwest A&F University; College of Water Resources and Architectural Engineering, Northwest A&F University, Yangling 712100, Shaanxi, China. Tel: +86-15209241621, Email: wangwene@nwafu.edu.cn.

al. (1974)[30] initiated the use of the ratio vegetation indices and the normalized difference vegetation indices to estimate crop characteristics. Subsequently, numerous vegetation indices (VIs) based on different combinations of wavelength reflectance have been developed for estimating leaf area index and soil and plant analyzer development. For example, Gitelson et al.[31] simply improved the NDVI to construct a new type of vegetation index: the wide dynamic range vegetation index ($WDRVI = (a\times\rho NIR-\rho Red)/(a\times\rho NIR+\rho Red)$), which increased the correlation with the vegetation indices and improved the estimation of high LAI by linearizing the relationship between typical wheat, soybean, and maize canopies. Borhan et al.[32] acquired spectral information of potato using a six-channel multispectral system at *R*, *G*, *B*, 550, 770, and 880 nm and verified that the multispectral band characteristics had a linear correlation with leaf chlorophyll of potato up to 0.95. Jay et al.[33] constructed a model of beet based on the vegetation indices and found that the vegetation indices constructed using only the spectra of the image elements of beet could enhance the sensitivity of chlorophyll content and leaf area index. Blancon et al.[34] monitored the dynamics of leaf area index of maize based on multispectral images of maize acquired by UAV, combined with high-throughput model-based methods, and successfully estimated the maximum leaf area index and leaf longevity.

However, relying solely on optical vegetation indices makes it difficult to accurately estimate both leaf area index and soil and plant analyzer development of winter wheat across multiple growth stages, especially during the later stages of wheat growth. The main problem is that spectral reflectance tends to saturate at high vegetation cover[35], and VIs often lose sensitivity during the reproductive phase[36]. Similar issues exist with vegetation indices extracted from RGB images, as these indices are calculated from the digital numbers of the red, green, and blue channels in color space transformations. Gray-Level Co-occurrence Matrix (GLCM) texture analysis, a potent image processing technique, quantifies spatial variability of adjacent pixel values within defined measurement windows[37], offering unique advantages in vegetation remote sensing. Variations in plant growth states, influenced by canopy three-dimensional morphology and structural heterogeneity, are effectively captured through texture feature alterations. This methodology has been widely applied to vegetation ecosystem monitoring, including biomass estimation[38,39], LAI retrieval[15], and vegetation coverage assessment[18]. Notably, integrated modeling combining spectral and GLCM texture features demonstrates superior performance. For instance, Zhang et al. (2021)[40] implemented the RF algorithm fusing texture and spectral features, achieving post-heading validation R^2=0.81 (RMSE=17.86%) with >20% accuracy improvement over vegetation index- or canopy index-based models. Similarly, Yue et al. (2019)[36] demonstrated that fusing ultra-high-resolution RGB texture features with vegetation indices improved winter wheat biomass estimation (R^2= 0.89, RMSE=0.82 t/ha), where texture features effectively resolved spectral saturation by characterizing vertical biomass distribution, reducing model errors by 22.63% during high-coverage stages. While these studies highlight the synergistic potential of GLCM texture-vegetation index fusion for crop parameter estimation and vegetation classification, existing research predominantly focuses on hyperspectral/multispectral imagery. Critical knowledge gaps persist in RGB-based estimation of winter wheat LAI and SPAD values through spectral-texture fusion approaches.

To incorporate the use of information from UAV remote sensing data, researchers explored different regression methods to determine quantitative relationships between remote sensing data variables and crop growth parameters. These regression methods can be classified into two main groups: 1) traditional linear regression techniques, including multiple linear regression[15], partial least squares regression[41], ridge regression[42], etc., and 2) machine learning algorithms covering back propagation neural networks[43], random forests[44], and support vector machines[45]. These methods are widely used in estimating crop traits due to 1) the strong correlation between VIs, TEs, and crop parameters, and 2) the ease of accessibility[21,37]. However, previous studies have tended to directly incorporate all feature variables extracted from remote sensing data into models, which increases the disparity between redundant or unrelated feature variables in high-dimensional data[46]. Moreover, severe multicollinearity problems between these variables can reduce the performance of the model and the interpretability of the model variables, prolonging the run time and reducing the overall efficiency[47,48]. Therefore, investigating feature selection or data dimensionality reduction and assessing whether the accuracy of the model can be maintained or improved after dimensionality reduction is of great importance[49].

In summary, the main content and contributions of this research are as follows:

1) Quantitative correlations between LAI, SPAD values, and remote sensing vegetation indices with texture features were analyzed across different growth stages of winter wheat.

2) The accuracy of models (MLR, RR, PLSR, BP, RF, and SVM) based on spectral indices, texture features, and their fusion for estimating LAI and SPAD in winter wheat was evaluated.

3) Feature selection and data downscaling methods (ST, PCA, ST_PCA) were used to reduce the number of explanatory variables in the model, and the potential of these methods was explored to improve the accuracy of LAI and SPAD estimation in winter wheat.

2 Materials and methods

2.1 Test area

The field is located in the Agricultural Demonstration Zone of Wugong Town, Xianyang City, Shaanxi Province (Figure 1). On October 18, 2022, two different genotypes of winter wheat (Xiaoyan 22 and Xinong 318) were sown. Two representative plots were selected for investigation, with control points placed around them. Trial site 1 consisted of 30 subplots, each measuring 8 meters in length and width, planting the genotype Xiaoyan 22 of winter wheat. Trial site 2 consisted of 20 subplots, measuring 10 meters by 8 meters, planting the genotype Xinong 318 of winter wheat. The experimental site is a flat terrain characterized by a semi-moist and arid climate with an average annual air temperature of 12.9°C, an average annual rainfall of 554 mm, and approximately 2162.4 h of annual sunshine. The soil type is clay loam with a pH of 8.14 and a dry weight of 1.48 g/cm^3, which makes it highly suitable for year-round rotation trials with wheat.

2.2 UAV image acquisition and ground experiments for LAI and SPAD measurement

The UAV remote sensing data collection was conducted during three crucial growth stages (jointing, heading, and grain filling) of winter wheat. The data acquisition period started at 12:00 PM and concluded at 2:00 PM (Table 1). A DJI Phantom 4 PRO quadcopter (SZ DJI Technology Co., Shenzhen, China) was used for aerial data acquisition, and the platform was equipped with a 1-inch CMOS sensor for a 20-megapixel camera. The UAV was automatically controlled by the DJI GS Pro Station application during the image acquisition process, with the camera pointed vertically downwards and set to fly at a speed of 5 m/s, an altitude of 80 m, and an overlap rate of 80% for both azimuth and elevation. The digital camera had an aperture of f/5 and a fixed ISO value of 100. The total number of wheat canopy images for each period was approximately 375, and the acquired UVA images were stitched using the Pix4D mapper software (www.pix4d.com), which aligned the photographs to the position orientation system (POS) using the WGS84 coordinate system.

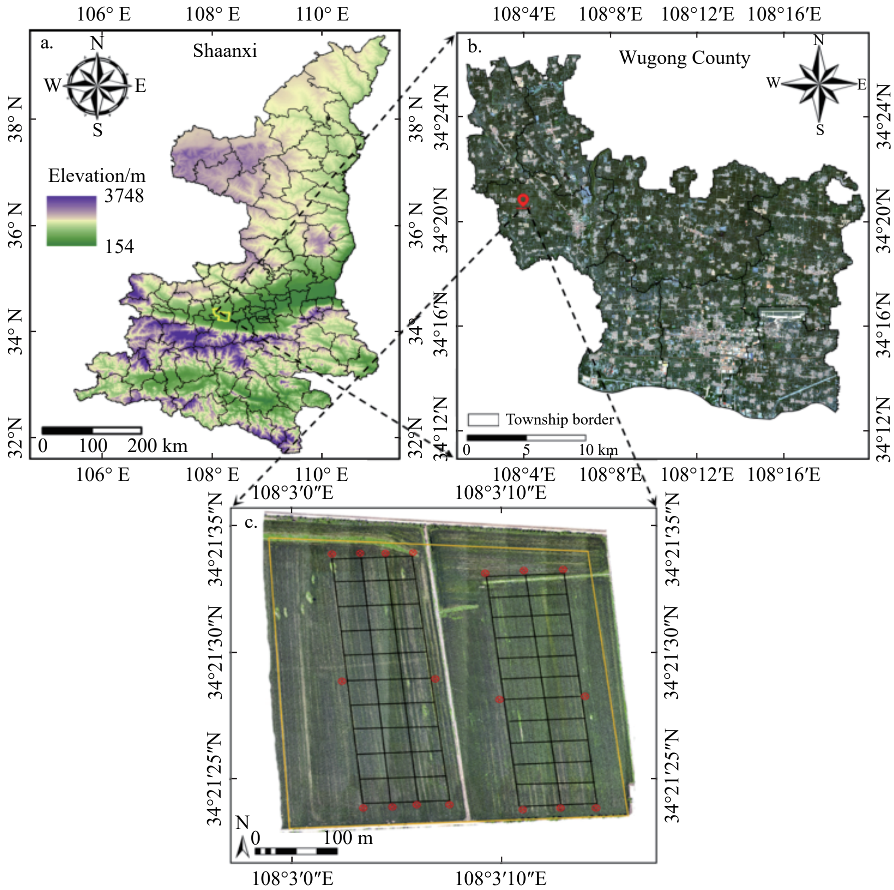

Figure 1 Location of the experimental site in this study

Table 1 Date of acquisition of UAV images and field data

Experiment	Test date	Growth stage	Number of aerial photos/Samples
Exp.1	2022.04.1	Joining stage	374/50
Exp.2	2022.05.1	Heading stage	375/50
Exp.3	2022.05.30	Filling stage	374/50

While obtaining UAV imagery, measurements of winter wheat's LAI and SPAD were conducted. In each subplot, 15 representative wheat plants were selected. The SPAD chlorophyll meter (Konika Minolta, Japan) was utilized to measure the chlorophyll content of the upper leaves of the wheat plants, and the mean value was taken as the specific test point's chlorophyll content. In the afternoon of the same day, the LAI and the average leaf inclination angle of the wheat were measured using a LAI 2200C (LI-COR, USA) with the probe mounted at 180° shade. The observed LAI values were read by sequentially measuring one time of zenith light and four times of under-leaf light under the wheat canopy, and the average value of three measurements was taken as the LAI value of each experimental point to minimize the error. The LAI values ranged from 1.24 to 4.43, and there was a total of two plots.

2.3 Selection and extraction of vegetation indices

The vegetation indices extracted from the RGB images are used to assess the growth status of the wheat, and 15 vegetation indices sensitive to leaf area index and chlorophyll are selected from previous studies. Regions of interest are delineated based on each experimental subplot, and the average digital number (DN) values of the three-color channels in the orthophoto image are calculated for each area of interest. The normalized values and vegetation indices are then calculated from the RGB data (Table 2).

Table 2 Bands and spectral vegetation indices calculated from UAV RGB imagery

Vegetation indices	Abbreviation	Formula	Reference
Normalized red index	r	$R/(R+G+B)$	
Normalized green index	g	$G/(R+G+B)$	
Normalized blue index	b	$B/(R+G+B)$	
Excess green index	EXG	2g–r–b	[50]
Excess green red index	EXR	1.4r–g–b	[51]
Visible atmospherically resistant index	VARI	$(G-R)/(G+R-B)$	[52]
Modified green red vegetation index	MGRVI	$(G^2-R^2)/(G^2+R^2)$	[53]
Normalized pigment chlorophyll index	NPCI	$(R-B)/(R+B)$	[54]
Color intensity index	INT	$(R+G+B)/3$	[55]
Woebbecke index	WI	(g–b)/(r–g)	[56]
Green red ratio index	GRRI	G/R	[57]
Normalized difference yellowness index	NDYI	$(G-B)/(G+B)$	[58]
Normalized green red difference index	NGRDI	$(G-R)/(G+R)$	[59]
Green leaf algorithm	GLA	$(2G+R-B)/(2G+R+B)$	[60]
Red green blue vegetation index	RGBVI	$(g^2-b\times r)/(g^2+b\times r)$	[53]

Note: In the formula, R, G, and B represent the reflectance of the red band, green band, and blue band, respectively.

2.4 Extraction of texture features

Texture features reflect homogeneous phenomena in an image, embodying structural arrangement properties of an object's surface that have slow transformations or periodic changes. Image texture is expressed by the grayscale distribution of pixels and their surrounding spatial neighborhood. Texture features extracted based on gray-level co-occurrence matrices have been widely used in estimating leaf area index, yield, and biomass[61–63]. GLCM extracts the relevant texture information of an image by considering the relative positions of pixels in the image and generating corresponding matrices to describe the spatial gray-level dependencies between image pixels[8,64]. In this study, eight texture features were calculated from RGB images using PyCharm 3.0. These features include mean (Mea), variance (Var), homogeneity (Hom), contrast (Con), dissimilarity (Dis), entropy (Ent), energy (Ene), and correlation (Cor). The texture features extracted by GLCM (such as contrast, entropy, and correlation) have significantly different value ranges, and directly inputting them into the model can lead to features with larger scales dominating the weight distribution. Therefore, the features are linearly mapped to [0, 1] using the formula TE = $(X_i–X_{min})/(X_{max}–X_{min})$, where TE is the texture feature of the i_{th} sample in the subsample image, and X_{max} and X_{min} are the highest and lowest values of the texture within the experimental area.

2.5 Data analysis and model development

The flowchart (Figure 2) depicts the experimental procedures, data processing, and methods of evaluation in this study. To obtain the LAI and SPAD estimation model for winter wheat at different growth stages, samples from three periods of jointing, tasseling, and filling were mixed as one dataset (n=150). 75% of the data were randomly selected as the calibration dataset and the rest (25% of the data) as the validation dataset. In this study, the performance of three linear regression models (MLR, RR, and PLSR) and three machine learning algorithms (BP, RF, and SVM) for LAI, SPAD estimation were compared by using vegetation indices, image texture, and a combination of the two, respectively. A tenfold cross-validation was used to compare the robustness of the different models. Coefficient of determination (R^2), root mean square error (RMSE), mean absolute error (MAE), and normalized root mean square error (NRMSE) were used to evaluate the performance of the models.

$$R^2 = 1 - \frac{\sum_{i=1}^{n}(O_i - P_i)^2}{\sum_{i=1}^{n}(O_i - \bar{O}_i)} \tag{1}$$

$$\text{RMSE} = \sqrt{\frac{1}{n}\sum_{i=1}^{n}(P_i - O_i)^2} \tag{2}$$

$$\text{NRMSE} = \frac{\text{RMSE}}{\max(O_i) - \min(O_i)} \times 100\% \tag{3}$$

$$\text{MAE} = \frac{1}{n}\sum_{i=1}^{n}|P_i - O_i| \tag{4}$$

where, O_i and P_i are the observed and estimated values (LAI or SPAD), respectively. $\bar{O}_i$ is the mean of the observed; and n is the number of samples.

Multiple linear regression (MLR) is a statistical method used to predict a dependent variable by simultaneously considering combinations of multiple independent variables. In this approach, it is essential to ensure a strong correlation between the independent

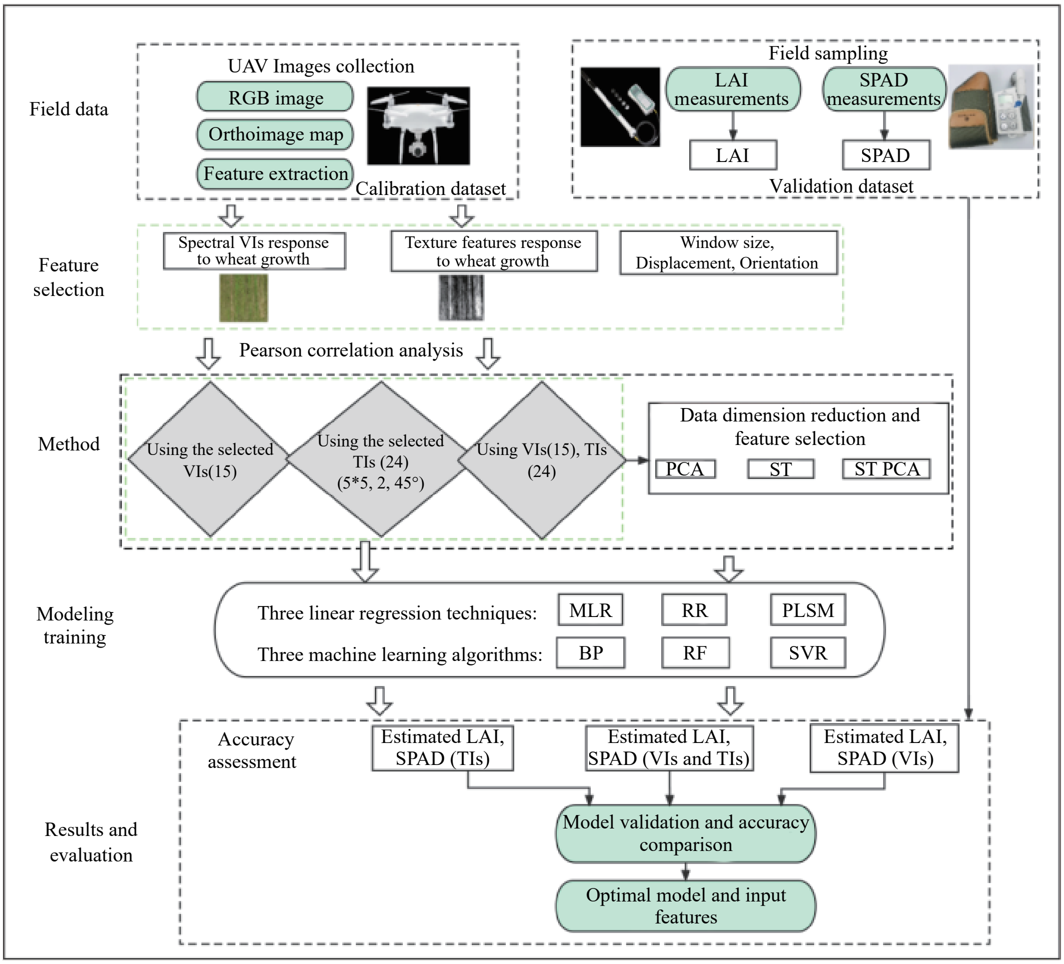

Figure 2 Flowchart of experimental methodology and statistical analysis

variables and the dependent variables to construct an effective regression model. The multiple linear regression model is typically represented as:

$$y = b_0 + b_1 x_1 + b_2 x_2 + \ldots + b_p x_p + \varepsilon \quad (5)$$

where, y is winter wheat biological parameters such as LAI and SPAD; b_0, b_1, ... , b_p are the regression coefficients; x_1, x_2, ..., x_p are the vegetation features derived from remote sensing data; ε is the random error.

Partial least squares regression (PLSR) is widely employed in various fields, including chemical analysis, drug development, and bioinformatics. Combining features of principal component analysis (PCA) and multiple linear regression, it effectively addresses common problems such as multicollinearity and overfitting that are often encountered in traditional linear models[65]. PLSR, which was originally proposed by Wold et al.[66], is used to uncover latent relationships between highly correlated predictor variables and the response variables, allowing the model to estimate the dependent variables using only a small number of independent variables.

Ridge regression (RR) is a modified least squares estimation approach that deliberately introduces bias into the estimates in exchange for better performance. It departs from the unbiasedness of ordinary least squares by accepting a trade-off between the loss of some information and a reduction in precision to obtain regression coefficients. Ridge regression is considered a more practical and reliable regression method, especially when dealing with data that may contain outliers, as it provides a better fit than ordinary least squares.

A backpropagation neural network (BP) is widely used to solve classification and regression problems and plays an important role in deep learning. The basic idea is to use the gradient descent method to find the partial derivatives of the objective function on the weights of each neuron layer by layer, which is used as the basis for updating the weights to make the model learn to achieve the desired performance[67]. In this paper, a BP model with five hidden layers is constructed with the mean squared error as the loss function, with a learning rate of 0.01, number of training iterations of 1000, and error threshold of 1×10^{-6}.

Random forest (RF) is a powerful machine learning algorithm that is widely used in various fields due to its accessibility and accuracy. RF is based on decision tree construction and improves model accuracy and robustness by combining multiple decision trees. Therefore, it is less sensitive to outliers and noise[62,68]. The number of decision trees and the number of observations per tree are two important parameters of RF models. A tenfold cross-validation approach was used to tune the RF model with the aim of finding the combination of hyperparameters that minimizes the RMSE. The optimal parameter values were then used for training the final regression model, and its performance on the test data was assessed by means of RMSE and MAE.

Support vector machine (SVM) is a powerful supervised learning algorithm used for classification and regression tasks, which is based on the principle of achieving classification by constructing a hyperplane that maximizes the distance between the learned samples[67]. SVM has many advantages, including efficient handling of high-dimensional data, powerful generalization capabilities, and good adaptability to nonlinear data. In this study, we introduced the radial basis function as the kernel function and used the grid search method and tenfold cross-validation to find the optimal penalty parameter C (4.0) and kernel parameter δ (0.8). As the independent variables have different scales and more dimensions between them, we performed normalization, scaling the independent variables to the range [−1, 1], and dimensionality reduction.

3 Results and analyses

3.1 Relationship between spectral features and in situ LAI, SPAD data

To establish the relationship between in situ measured LAI, SPAD, and spectral features of wheat, Pearson's correlation coefficients were calculated between 15 spectral indices derived from the UAV RGB images and the relationships with LAI and SPAD (Figure 3). The results indicated that there were significant correlations between most of the spectral indices. Among them, the most significant vegetation indices correlations were found between NGBDI and GLA (R=0.99) with RGBVI and NDVI (R=0.98). The correlations between spectral indices and LAI or SPAD differed at various growth stages. In estimating LAI, the best performing VIs were GRRI (R=0.63), GLA (R=0.50), and MGRVI (R=0.48) at the jointing, tasseling, and filling stages, respectively. For SPAD estimation, the best-performing VIs during these stages were R (R=−0.89), NPCI (R=−0.71), and GLA (R=−0.63), respectively. Overall, spectral indices perform better in monitoring SPAD compared to LAI. In addition, it was found that the correlation between LAI, SPAD, and spectral indices characteristics decreased using data from all stages.

3.2 Relationship between texture features and in situ LAI, SPAD data

To further investigate the relationship between texture features extracted from RGB images and wheat LAI and SPAD, Pearson correlation coefficients between eight image texture features, calculated based on a 5×5 window, 45° orientation, and 2-pixel displacement, and LAI and SPAD were compared (Figure 4). The results indicated that for a single growth stage, most texture features had weak correlations with LAI (R values ranged from 0.09 to 0.32) and SPAD (R values ranged from 0.05 to 0.39). However, when analyzing textural characteristics covering three different growth stages, the correlations increased significantly; for LAI, R values varied from 0.17 to 0.43 and for SPAD from 0.11 to 0.48. Furthermore, it was also observed that the texture variables in the red band outperform those in the green and blue bands in terms of their correlation with LAI and SPAD. Specifically, for LAI, the highest correlation was observed with the red band entropy (Ent), R from 0.28 to 0.43, followed by the red band energy (Ene), R from 0.20 to 0.41. In terms of SPAD, Dis exhibited the highest correlation (R=0.48), followed by Cor (R=0.45). It is noteworthy that, except for Mea, Var, and Cor, most of the texture features from the jointing stage scored better in terms of their correlations with LAI and SPAD compared to the heading and filling stages. These characteristics include Hom, Con, Dis, Ent, and Ene.

3.3 LAI and SPAD estimation models constructed using spectral vegetation indices

The relationship between the estimated values from the regression model based solely on vegetation indices and the field measurements are shown in Figures 5 and 6. In most cases, the accuracy of linear regression models was found to be lower than that of machine learning models. For LAI estimation, R^2 values for linear models ranged between 0.52 and 0.63, while machine learning models achieved R^2 values between 0.57 and 0.74. For SPAD estimation, linear models showed R^2 values ranging from 0.57 to 0.65, while machine learning models showed R^2 values from 0.68 to 0.82. Among the linear regression models used for LAI estimation, the MLR model outperformed others with R^2 values ranging from 0.58 to 0.63, and the RMSE values ranged from 0.45 to 0.53, and the MAE values varied from 0.36 to 0.42. Among the machine learning models, the RF model showed the highest accuracy in LAI estimation. RF achieved higher R^2 values compared to the BP and SVM models and displayed relatively lower RMSE and MAE. For SPAD estimation, the MLR model performed best among the three linear regression models with R^2=0.63, RMSE=3.20, and MAE=2.60 for the calibration dataset and R^2=0.65, RMSE=3.14, and MAE=2.58 for the validation dataset. The RF model also provided superior results among the three machine learning models, with R^2=0.82, RMSE=2.15, and MAE=1.67 for the calibration dataset, and R^2=0.76, RMSE=3.04, and MAE=2.58 for the validation dataset. Furthermore, the scatterplots indicated that estimation models relying solely on spectral vegetation indices generally tend to underestimate samples with high LAI and SPAD values. Establishing multi-stage LAI and SPAD estimation models based on spectral vegetation indices alone is challenging.

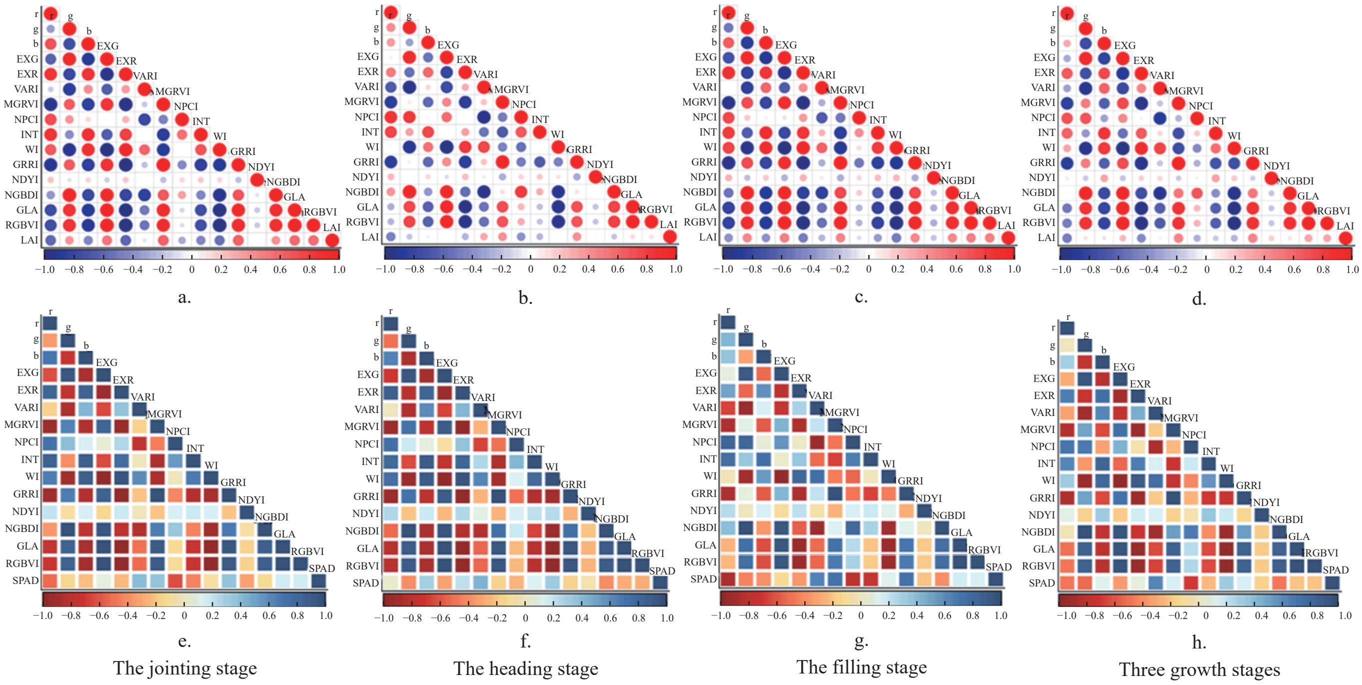

Figure 3 Correlation analysis between RGB image spectral indices and LAI, SPAD at different growth stages

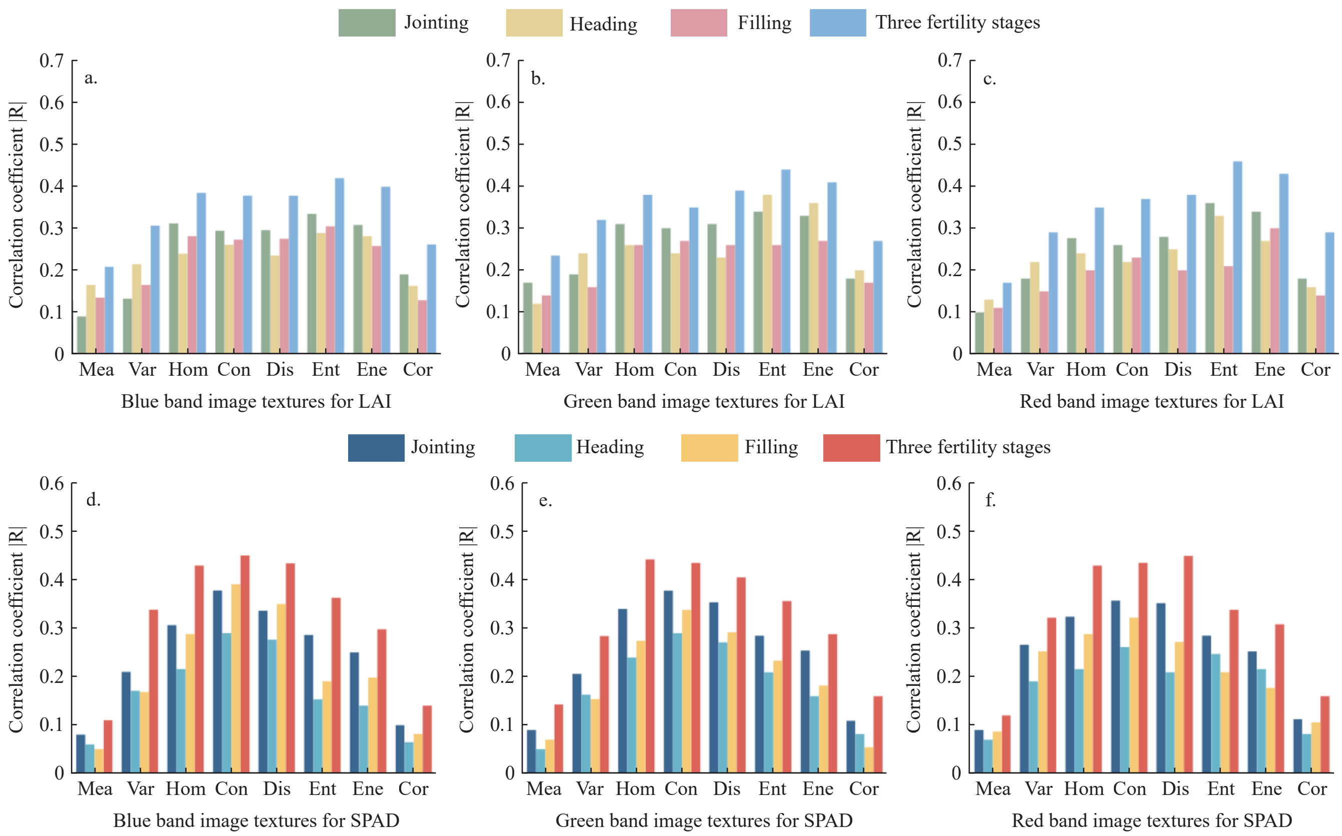

Figure 4 The relationship between image texture features and LAI and SPAD of winter wheat at different growth stages

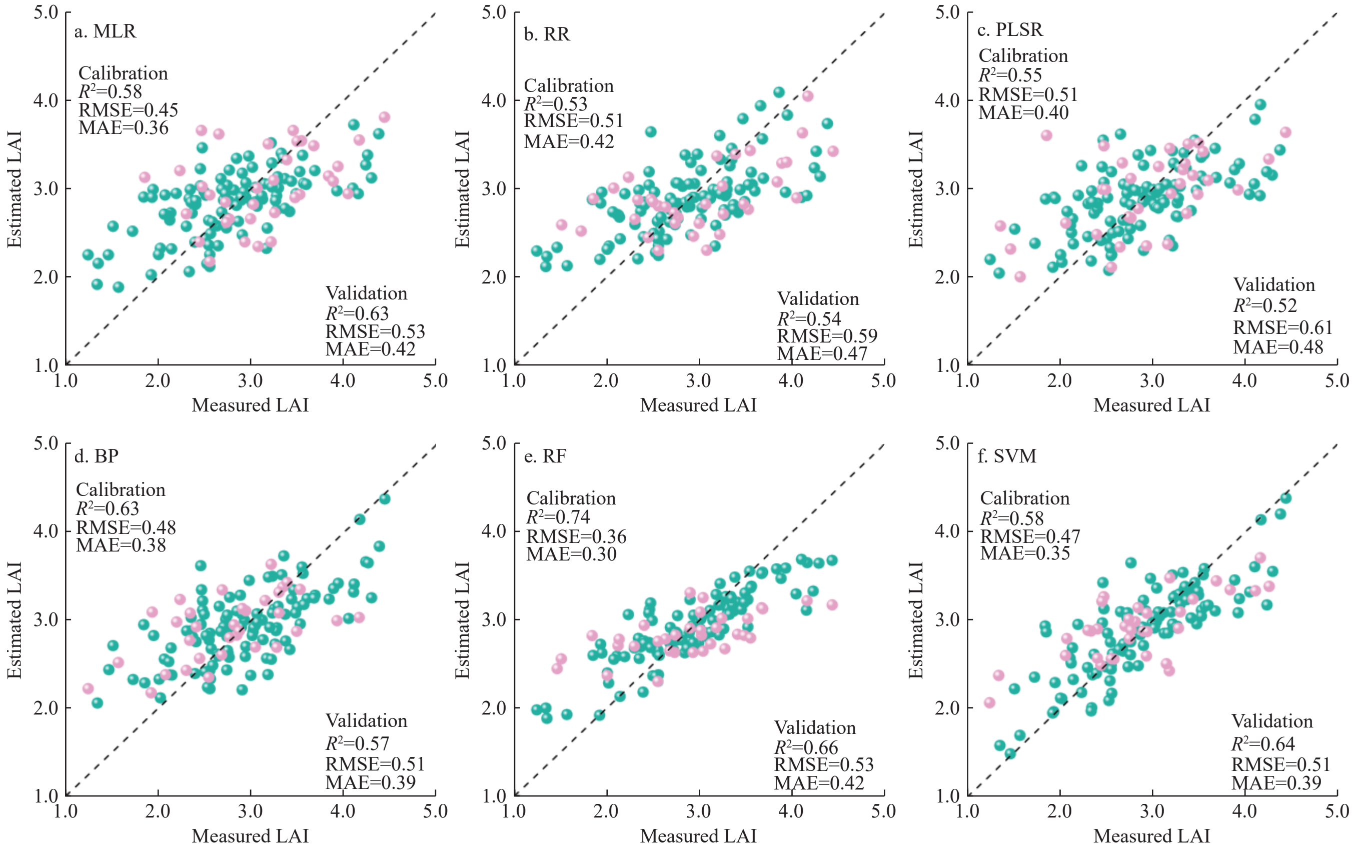

Note: Three linear regression models: MLR, RR, and PLSR; three machine learning models: BP, RF, and SVM. The same below.

Figure 5 Winter wheat LAI estimation models established using only vegetation indices

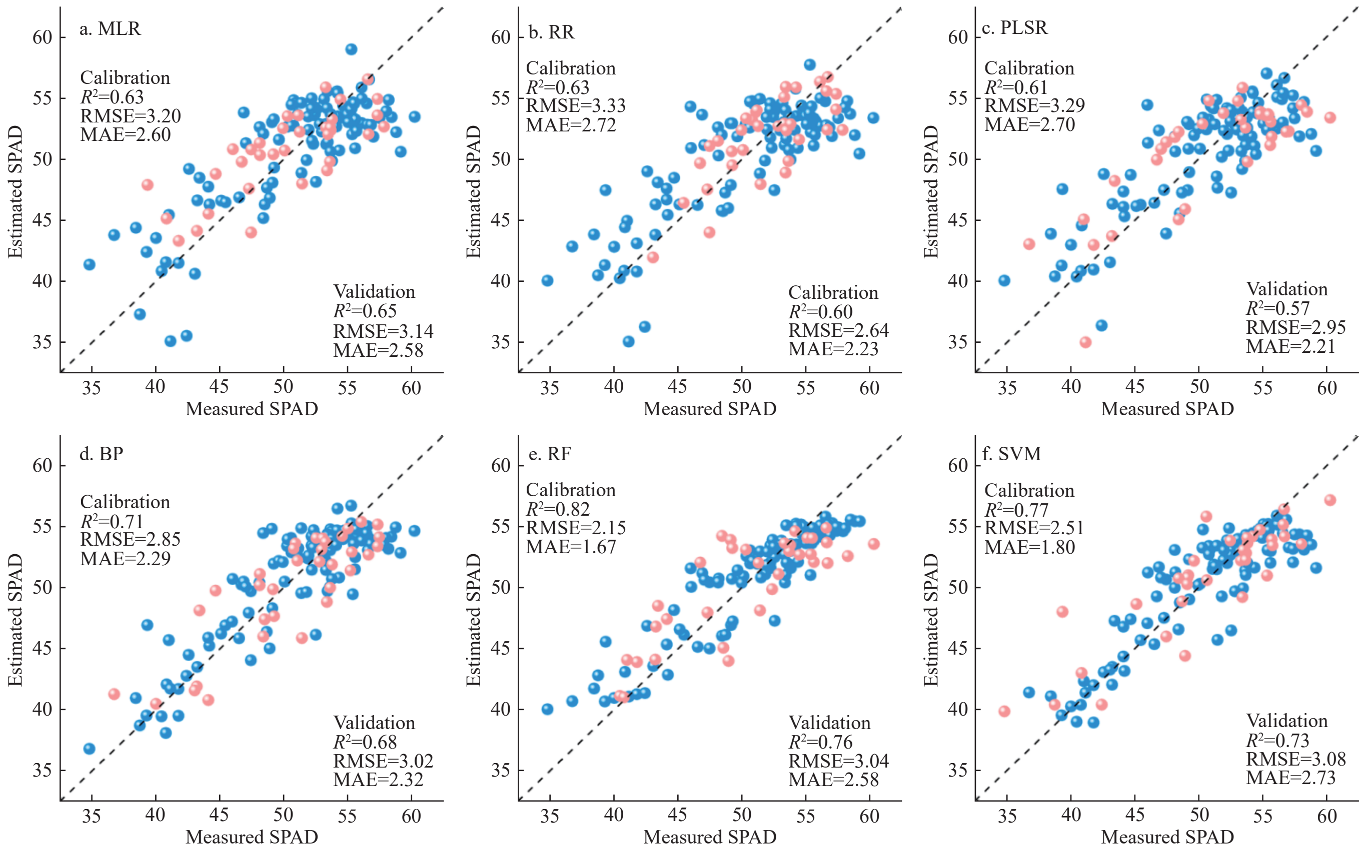

Figure 6 Winter wheat SPAD estimation models established using only vegetation indices

3.4 LAI and SPAD estimation models constructed using RGB image textures

Six regression models for leaf area index and soil and plant analyzer development were individually established based on the extraction of texture features from different bands of RGB images, consisting of three linear regression models (MLR, RR, and PLSR) and three machine learning models (BP, RF, and SVM). The selected image bands, window sizes, displacements, and texture features are presented in Table 3. The results (Table 4) demonstrated that among the six different estimation models, for LAI estimation, the RF and SVM models had higher R^2 values (ranging from 0.52 to 0.57) and relatively lower RMSE (ranging from 0.42 to 0.47) and MAE (ranging from 0.31 to 0.37) compared to other models. For SPAD estimation, the RF model performed best with R^2 greater than 0.56, RMSE less than 2.96, and MAE less than 3.5, followed by the SVM model, which also performed relatively well (R^2≥0.53, RMSE≤3.14, and MAE≤2.43). In summary, the use of image texture alone to construct LAI and SPAD estimation models has low accuracy.

Table 3 Selected optimal GLCM-based structure parameters for estimating LAI and SPAD in winter wheat

Types	Image bands	Windows sizes	Displacements	Angles	Texture features
GLCM-based textures	Three bands of the RGB image: B, G, and R	5 × 5	2 pixels	45° orientation	Mea, Var, Hom, Con, Dis, Ent, Ene, Cor, a total of 24 features

Table 4 Estimation results of winter wheat LAI and SPAD from different regression models established using only vegetation indices

Index	Experiments	LAI						SPAD					
		MLR	RR	PLSR	BP	RF	SVM	MLR	RR	PLSR	BP	RF	SVM
R^2	Calibration	0.52	0.41	0.39	0.48	0.55	0.53	0.53	0.52	0.47	0.49	0.58	0.55
	Validation	0.49	0.37	0.44	0.43	0.57	0.52	0.51	0.43	0.41	0.47	0.56	0.53
RMSE	Calibration	0.42	0.47	0.51	0.48	0.44	0.45	3.03	3.28	3.21	3.26	2.82	3.03
	Validation	0.47	0.52	0.50	0.52	0.42	0.47	3.30	3.47	3.48	3.35	2.96	3.14
NRMSE/%	Calibration	13.17	14.73	15.99	15.05	13.64	14.26	12.45	13.48	13.19	13.40	11.57	12.45
	Validation	14.73	16.30	15.67	16.30	13.18	14.88	13.56	14.26	14.30	13.77	12.13	12.91
MAE	Calibration	0.32	0.39	0.42	0.39	0.35	0.33	2.36	2.47	2.41	2.45	2.26	2.37
	Validation	0.35	0.40	0.53	0.44	0.31	0.37	2.41	2.54	2.67	2.52	2.35	2.43

3.5 LAI and SPAD estimation models constructed by fusing spectral vegetation indices and textural features

Three linear regression models and three machine learning models were compared based on the fusion of 24 texture features (TEs) and 15 vegetation indices (VIs). The results showed that the combined use of texture features and vegetation indices could effectively improve the estimation accuracy of LAI and SPAD models compared to models based on only vegetation indices or texture features (Figures 7 and 8). For LAI estimation, the R^2 values of the three linear regression models ranged from 0.67 to 0.74, with RMSE values from 0.32 to 0.42 and MAE values from 0.26 to 0.34. Among these models, the MLR model obtained the best performance. In the case of machine learning techniques, both RF and SVM showed relatively high performance. However, it is worth noting that the RF model had a lower RMSE (0.31) and MAE (0.25) on the validation dataset. For SPAD estimation, the linear regression model with optimal performance was MLR (calibration dataset R^2=0.75, RMSE=2.81, MAE=2.24; validation dataset R^2=0.79, RMSE=2.67, MAE=2.04), and the optimal machine learning model was RF (calibration dataset R^2=0.88, RMSE=2.23, MAE=1.73; validation dataset R^2=0.85, RMSE=2.52, MAE=2.02). The changes in wheat in different growth stages could be reflected by textural features. After wheat enters the tillering stage, the leaves obscure most of the soil background, and the change in vegetation indices decreases, which easily leads to the underestimation of LAI and SPAD (Figure 5). By fusing image texture features and vegetation indices to estimate LAI and SPAD, this underestimation condition was mitigated (Figure 6) and the accuracy of the models was improved.

3.6 Feature importance of LAI and SPAD estimation models

To further evaluate the performance of the optimal estimation models for LAI and SPAD, we conducted a feature importance analysis (Figure 9). For LAI estimation based on vegetation indices, EXR and r exhibited the highest importance, with contribution rates of 0.77 and 0.60, respectively. In SPAD estimation, NOCI and VARI were the primary driving factors, effectively suppressing soil background interference and accurately capturing the spatial variability of leaf chlorophyll content. Texture feature analysis revealed that Var and Ent were the key texture indicators for LAI estimation. In SPAD estimation, Mea and Con were particularly significant. The feature fusion model demonstrated cross-modal synergistic effects (Figures 9e and 9f). In LAI estimation, the interactive contributions of Var, VARI, and NDVI were relatively high, with values of 0.83, 0.50, and 0.40, respectively. For SPAD estimation, NDVI and NPCI had the highest contributions, at 0.83 and 0.51, respectively. These findings indicate that the fusion of vegetation indices and texture features is not merely a simple combination but rather an integration that leverages spectral and spatial complementarity, overcoming the limitations of single data sources in representation.

3.7 Impacts on the accuracy of the LAI, SPAD estimation model of different data dimensionality reduction methods

3.7.1 Features selection

Multicollinearity between vegetation indices and texture features posed a significant threat to model stability and generalization performance and reduced the statistical significance of model variables[62]. Principal component analysis (PCA) and stepwise selection (ST) dimensionality reduction methods were used to address this issue. PCA was performed on the feature matrix and eigenvalues, in which the contribution rates of the first four principal components were 57.51%, 31.27%, 6.86%, and 3.17%, with a cumulative contribution of 98.81% for VIs. For TEs, the contribution rates of the first five principal components were 80.56%, 7.38%, 4.74%, 2.13%, and 1.75%, with a cumulative contribution of 96.56% (as listed in Table 5). When considering both VIs and TEs (VIs+TEs), the cumulative contribution of the first six principal components reached 95.48%. In all these cases, the cumulative contribution rate of the PCA was above 95%, which indicated that the selected components were sufficient to explain most of the information in all the data columns.

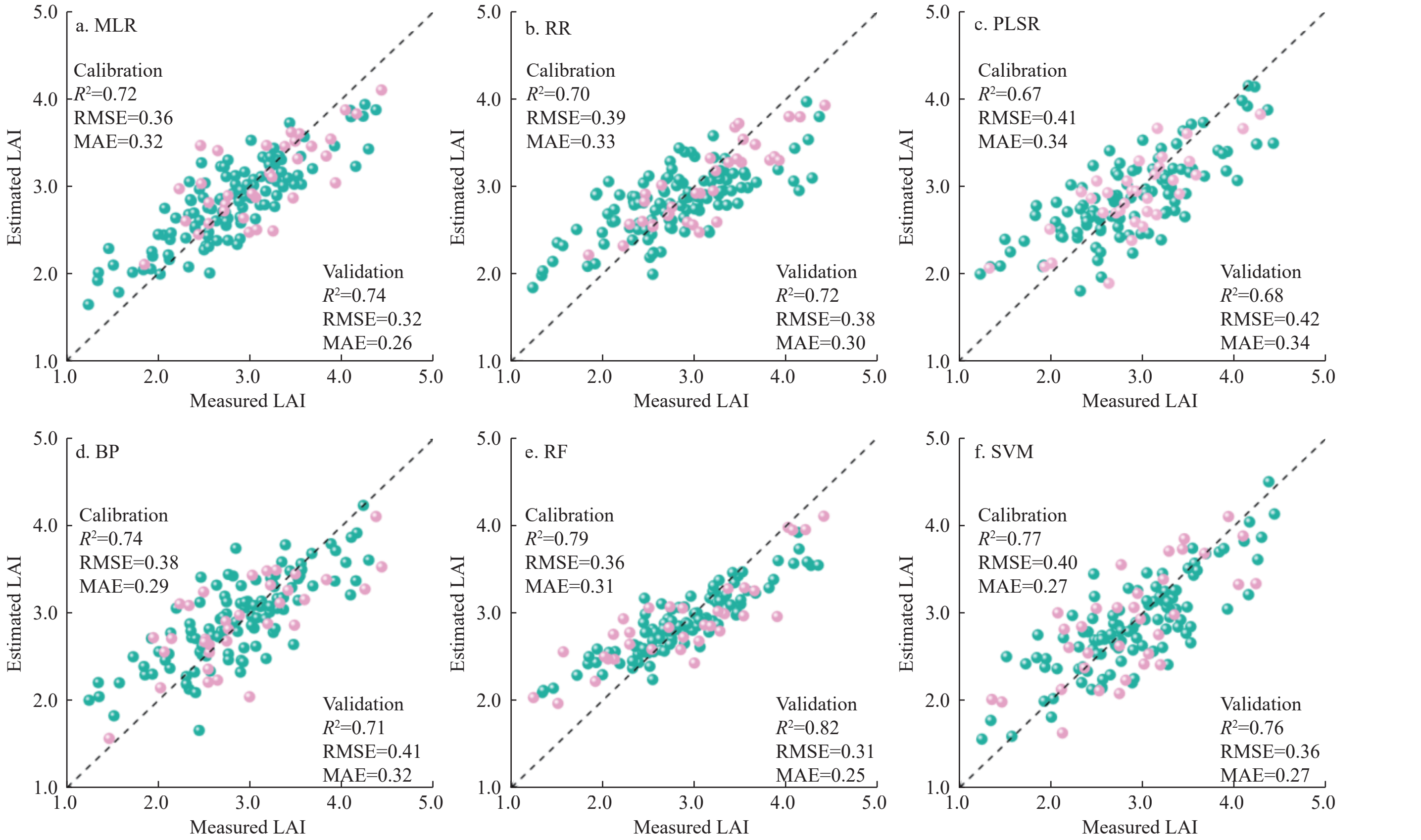

Figure 7 Winter wheat LAI estimation models established by fusing the vegetation indices and image texture

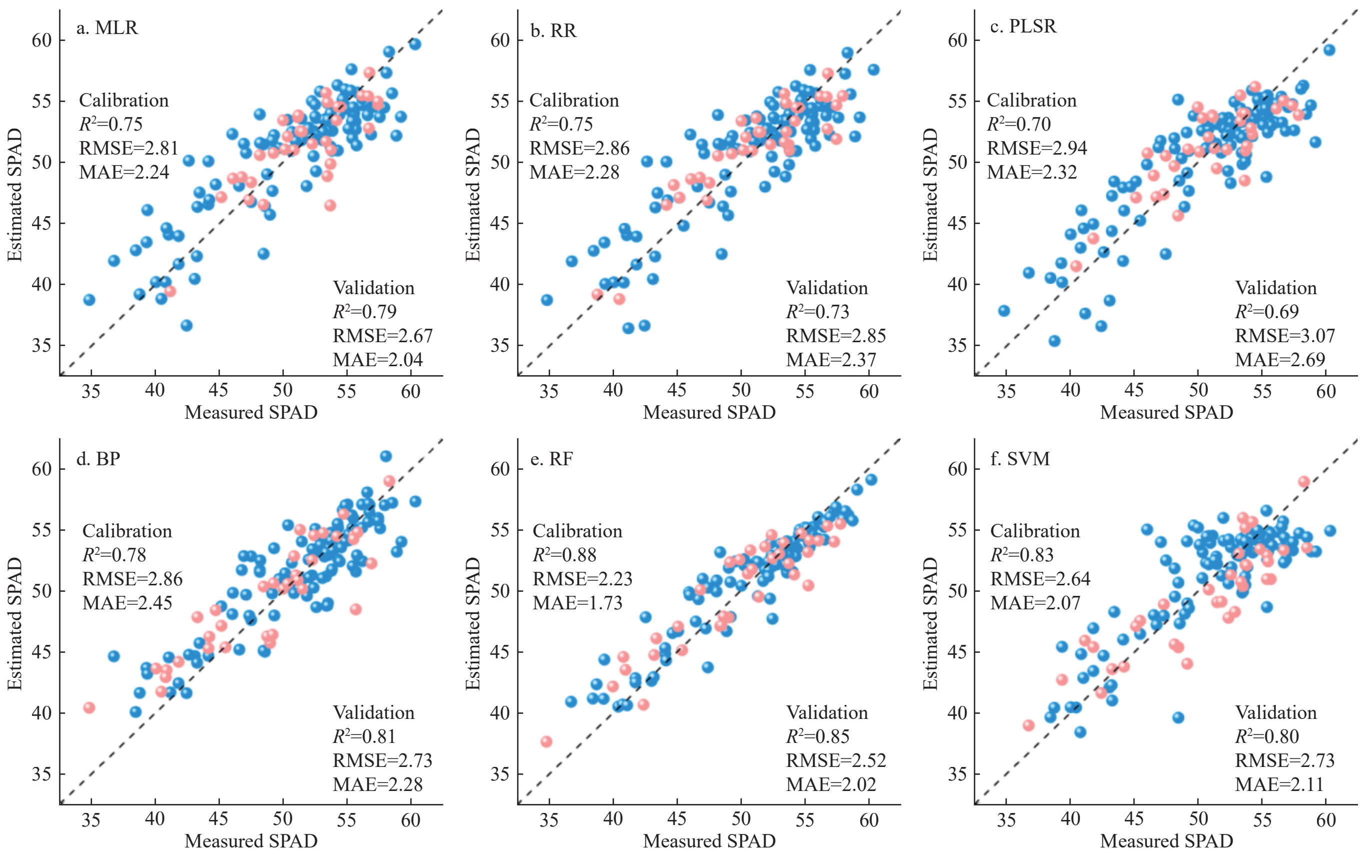

Figure 8 Winter wheat SPAD estimation models established by fusing the vegetation indices and image texture

3.7.2 Comparison of model performance with different feature selection methods

The performance of linear regression and machine learning models combined with PCA is listed in Table 6. Compared to models without data dimensionality reduction or feature selection, the regression models established incorporating PCA have shown improved performance along with reduced model complexity and computational load. When estimating LAI using VIs as the input set, the PCA-RF model (R^2=0.72, RMSE=0.31, NRMSE=9.72%, MAE=0.25) achieved the best accuracy using seven components. Compared to models without data dimensionality reduction, it showed a 4.35% increase in R^2, along with an 11.43% reduction in RMSE and a 10.71% reduction in MAE. When using VIs+TEs as the input set, R^2 increased from 2.82% to 5.19%, RMSE decreased from 5.00% to 14.71%, and MAE decreased from 2.78% to 14.29%.

When estimating SPAD using VIs as the input set, both the PCA-RF and PCA-SVM models showed high accuracy (R^2≥0.75). Compared to models without data dimensionality reduction, the R^2 increased by 5.06% and 3.85%, and the NRMSE decreased by 3.68% and 2.43% for the PCA-RF and PCA-SVM models, respectively. The estimation results of PCA combined with different regression models indicated that PCA is effective in reducing the number of predictors needed to build models while maintaining model accuracy.

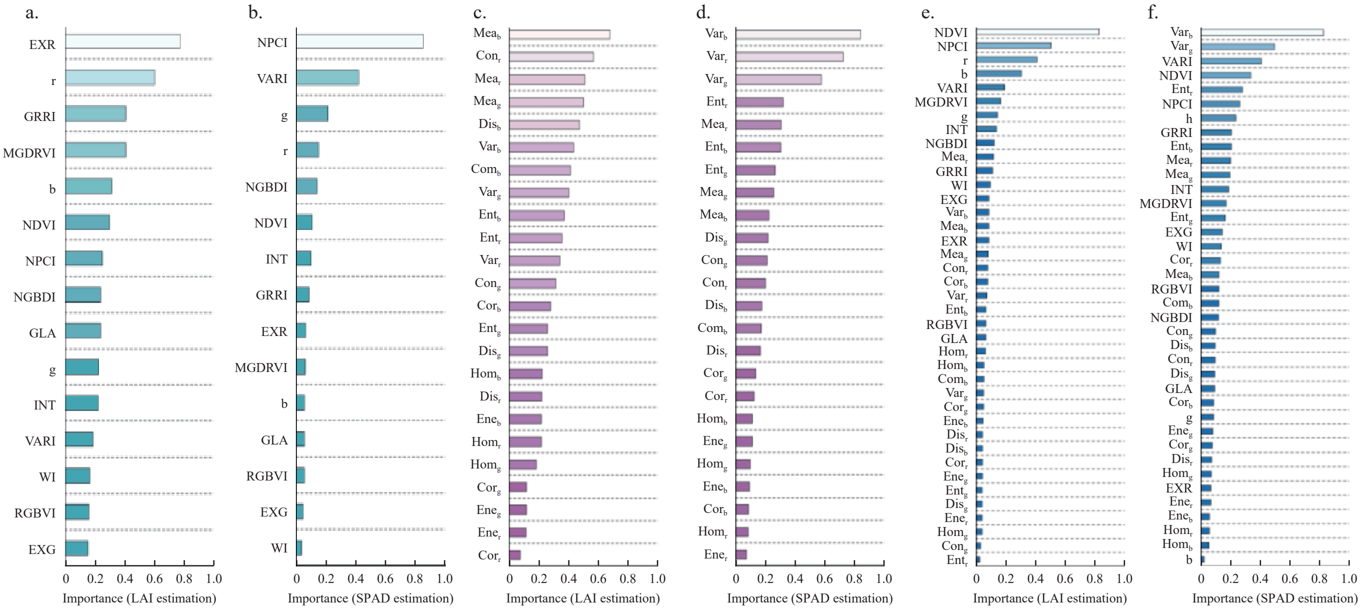

Figure 9 Ranking of feature importance for winter wheat LAI and SPAD (a. b. Vegetation index models; c. d. Texture feature models; e. f. Multi-feature fusion models)

Table 5 Contributions of PCA components with different input sets

Components	VIs	TEs	VIs+TEs
1	57.51%	80.56%	50.22%
2	31.27%	7.38%	23.90%
3	6.86%	4.74%	12.23%
4	3.17%	2.13%	4.27%
5	0.14%	1.75%	3.05%
6	0.03%	1.10%	1.81%
Total	99.25%	97.66%	95.48%

Stepwise regression (ST) was used to construct an optimal predictive model by gradually adding or removing features. The results of the ST approach combined with different models for estimating LAI and SPAD in winter wheat are presented in Table 7. When ST-VIs and ST-TEs were used as independent inputs to the dataset to estimate LAI and SPAD in wheat, there was no improvement in the accuracy of the three linear models and even a decreasing tendency (MLR) compared to the model without feature selection. However, when ST-VIs+TEs were used as inputs to estimate LAI and SPAD in wheat, the accuracy of the six regression models was improved to some extent, with R^2 increasing from 0.70% to 3.65%. In particular, the accuracy of the machine learning models (RF, SVM) was significantly improved, with R^2 increasing from 2.53% to 3.65%, indicating that ST was able to effectively filter the multifactorial variables[39].

The ST_PCA method was adopted to enhance the model accuracy. Different data dimensionality reduction or feature selection methods (PCA, ST, ST_PCA) combined with six

Table 6 Estimation results based on PCA combined with different models using three input sets

Accuracy	Input set	LAI estimation models VIs	LAI TEs	LAI VIs+TEs	SPAD estimation models VIs	SPAD TEs	SPAD VIs+TEs
R^2	MLR	0.64	0.56	0.73	0.68	0.55	0.75
	RR	0.59	0.43	0.70	0.63	0.49	0.72
	PLSR	0.57	0.44	0.67	0.59	0.48	0.67
	BP	0.64	0.48	0.75	0.69	0.53	0.81
	RF	0.72	0.61	0.83	0.79	0.61	0.86
	SVM	0.69	0.56	0.81	0.75	0.58	0.84
RMSE	MLR	0.36	0.35	0.31	2.94	2.72	2.55
	RR	0.41	0.41	0.36	2.78	2.99	2.61
	PLSR	0.44	0.47	0.38	3.10	3.05	2.92
	BP	0.38	0.43	0.36	2.82	3.11	2.71
	RF	0.31	0.32	0.29	2.34	2.40	2.07
	SVM	0.35	0.35	0.31	2.62	2.51	2.56
NRMSE/%	MLR	11.29	11.04	9.72	12.07	11.18	10.46
	RR	12.85	12.88	11.29	11.44	12.29	10.73
	PLSR	13.79	14.72	11.91	12.76	12.54	11.99
	BP	11.91	13.50	11.29	11.59	12.78	11.12
	RF	9.72	10.12	9.09	9.62	9.86	8.51
	SVM	10.97	11.04	9.72	10.76	10.32	10.54
MAE	MLR	0.30	0.28	0.26	2.11	1.92	1.96
	RR	0.33	0.32	0.31	2.43	2.11	2.10
	PLSR	0.36	0.40	0.35	2.50	2.38	2.33
	BP	0.29	0.38	0.27	2.11	2.26	1.96
	RF	0.25	0.25	0.24	1.90	1.83	1.80
	SVM	0.28	0.27	0.25	2.04	1.91	1.92

regression models yield LAI and SPAD estimation results as shown in Figure 10. For the three linear regression models (MLR, RR, and PLSR), ST_PCA hurts LAI and SPAD estimation using VIs and TEs as input datasets. In contrast to the performance with linear regression models, the combination of ST_PCA with three machine learning models effectively improves the model accuracy, especially when VIs+TEs are employed as the input set. ST_PCA combined with RF and SVM shows better performance (R^2=0.86, RMSE=0.26, MAE=0.22 for LAI estimation; R^2=0.91, RMSE=2.01, MAE=1.66 for SPAD estimation).

Table 7 Estimation results based on ST combined with different models using three input sets

Accuracy	LAI estimation models				SPAD estimation models		
	Input set	VIs	TEs	VIs+TEs	VIs	TEs	VIs+TEs
R^2	MLR	0.60	0.52	0.72	0.65	0.51	0.74
	RR	0.56	0.39	0.69	0.61	0.43	0.70
	PLSR	0.54	0.41	0.65	0.58	0.42	0.66
	BP	0.62	0.47	0.73	0.66	0.47	0.79
	RF	0.71	0.57	0.82	0.76	0.56	0.86
	SVM	0.68	0.53	0.79	0.73	0.54	0.83
RMSE	MLR	0.42	0.42	0.34	3.05	2.97	2.50
	RR	0.43	0.48	0.37	2.83	3.24	2.60
	PLSR	0.45	0.50	0.39	3.16	3.32	2.81
	BP	0.41	0.45	0.37	2.85	3.10	2.73
	RF	0.33	0.38	0.30	2.49	2.70	1.87
	SVM	0.36	0.42	0.33	2.70	2.91	2.64
NRMSE/%	MLR	13.17	13.24	10.66	12.54	12.21	10.29
	RR	13.48	15.05	11.60	11.64	13.32	10.67
	PLSR	14.11	15.83	12.23	12.97	13.65	11.56
	BP	12.85	14.03	11.60	11.71	12.74	11.20
	RF	10.34	11.98	9.40	10.23	11.10	7.69
	SVM	11.29	13.26	10.34	11.10	11.96	10.84
MAE	MLR	0.32	0.35	0.27	2.21	2.25	2.04
	RR	0.35	0.38	0.32	2.46	2.39	2.30
	PLSR	0.36	0.45	0.36	2.54	2.50	2.35
	BP	0.30	0.41	0.29	2.12	2.32	1.99
	RF	0.27	0.31	0.24	1.95	2.12	1.86
	SVM	0.29	0.33	0.27	2.08	2.23	1.97

4 Discussion

4.1 Feasibility of LAI, SPAD estimation using spectral vegetation indices derived from UAV RGB images

The estimation of leaf area indices and chlorophyll content relies mainly on satellite data and multi-sensor UAV[69]. However, both of these methods have limitations in field trials. Satellites are often limited by revisit periods and weather conditions, making it difficult to provide sufficiently effective data at critical stages of crop growth. Multiple sensors, such as multispectral and hyperspectral sensors, can capture a wealth of information, but storing and processing this data is not straightforward and can easily lead to data redundancy and wastage[42,70-72]. The collection of RGB images by UAV is simple, economical, and easy to process[73]. In this study, six LAI and SPAD estimation models for winter wheat were developed by selecting 15 commonly used vegetation indices, and the results showed that the machine learning algorithm model had superiority in LAI and SPAD estimation for multiple fertility stages of winter wheat, compared to the linear regression model. The R^2 of the linear regression model ranged from 0.52 to 0.65, and the R^2 of the machine learning model ranged from 0.57 to 0.82. This is similar to the findings of Ma et al.[42], who used machine learning techniques and linear regression models to monitor cotton yield by integrating vegetation indices from RGB images. Zhang et al.[64] also found that the machine learning RF method has a more robust capability than MLR in terms of handling different remote sensing indices when estimating crop growth parameters using UAV, which further reduced the RMSE from 2.74% to 5.11% in the estimation of LAI. However, estimating LAI, SPAD at multiple growth stages using RGB optical vegetation indices has drawbacks and limitations[36,63]: 1) vegetation indices features of crops are easily obscured or saturated under high canopy cover, e.g. correlation of spectral indices with LAI, SPAD was significantly lower at multiple growth reproductive stages (Figure 3); 2) parameters of later growth stages are mostly underestimated, e.g. high LAI, SPAD samples

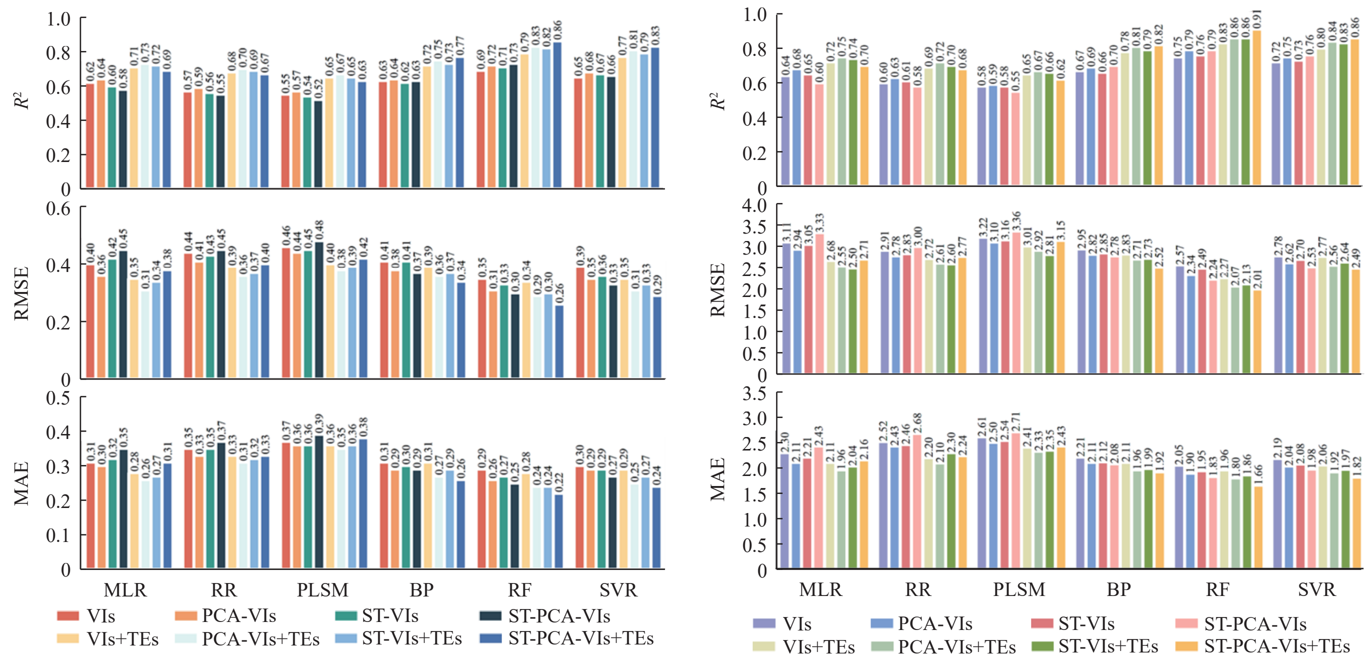

a. LAI estimation based on feature selection

b. SPAD estimation based on feature selection

Figure 10 Tenfold cross-validated R^2, RMSE, and MAE of regression models for winter wheat LAI and SPAD estimations were underestimated in all six models (Figures 5 and 6). In other studies, Bendig et al.[53] also reported methods based on spectral vegetation indices and that SPAD data were widely underestimated in the later crop growth stages. Estimation of crop parameters relying solely on optical vegetation indices remains challenging, and new methods are required to improve the accuracy of crop parameter estimation at multiple growth stages[35].

4.2 Estimation of LAI and SPAD by fusion of vegetation indices and texture features from UAV RGB images

The performance evaluation based on texture features (24 TEs) and vegetation indices (15 VIs) extracted from RGB images in estimating winter wheat LAI and SPAD showed that the estimation accuracy using only texture features (Table 4) was lower than that using vegetation indices. In assessing aboveground biomass (AGB) in winter oilseed rape fields, Duan et al.[74] found single texture indices less accurate than vegetation indices (VIs). Furthermore, research conducted by Guo et al.[75] revealed that vegetation indices significantly outperformed texture characteristics in monitoring wheat yellow rust and estimating wheat biomass. Nevertheless, it is undeniable that texture features play an important role in estimating physiological and biochemical parameters of crops. Texture features, which primarily contain spatial information, are unaffected by the brightness or color of the observed crop surface and reflect the grayscale data, spatial variations, and structural information of the image. In contrast, spectral indices indicate the biochemical properties of the canopy leaves. Texture features and spectral indices respond differently to canopy structural characteristics and are complementary. Our research also provides evidence that the combined use of spectral and textural features extracted from RGB images significantly improves the estimation accuracy of LAI and SPAD, compared to using single optical indices or image texture features. Specifically, the integrated image texture largely eliminated the underestimation of high LAI values (3.5-5.0) and SPAD values (55-60) (Figures 7 and 8). In other studies, Reddersen et al.[76] reported that methods based on spectral VIs underestimate higher AGB values, while new indicators such as texture information and canopy structure modeling (CSM) techniques could avoid this underestimation. Yuan et al.[77] demonstrated that integrating eight GLCM texture features with spectral parameters significantly improved rice LAI estimation accuracy. The fused texture-spectral SVM-POA model enhanced validation R^2 from 0.839 to 0.917, reduced RMSE by 69.8%, and decreased MAE to 4.91%. Texture features effectively captured canopy structural information and mitigated spectral saturation issues, particularly during high-density canopy phases such as the jointing and heading stages.

4.3 Comparison of data dimensionality reduction methods combined with different regression models for LAI, SPAD estimation

This study compared the performance of three linear regression techniques (MLR, RR, and PLSR) and three machine learning algorithms (BP, RF, and SVM) with spectral indices, texture features, and their combinations extracted from UAV RGB images. Machine learning algorithms consistently outperform linear regression models in estimating LAI and SPAD. Even the best-performing linear regression model (MLR-VIs+TEs, calibration dataset: R^2=0.75, RMSE=2.81, MAE=2.24; validation dataset: R^2=0.79, RMSE=2.67, MAE=2.04) exhibited lower accuracy compared to the worst-performing machine learning model (BP-VIs+TEs, calibration dataset: R^2=0.78, RMSE=2.86, MAE=2.45; validation dataset: R^2=0.81, RMSE=2.73, MAE=2.28). Machine learning algorithms have been demonstrated to possess robust capabilities for handling non-linear and multivariate regression between remote sensing data and vegetation physiological and biochemical parameters[42,78]. The RF model performed better than the SVM model among the three machine learning models, while the BP model was the weakest in all three types of data inputs. This was consistent with the view of Wu et al.[15], who used random forest, support vector machine, and multiple linear regression techniques to fuse spectral, structural, and thermal characteristics of the canopy to estimate LAI in wheat, and revealed that RF performed best in LAI prediction, regardless of which features were fused. Zha et al.[79] also found that RF was superior to SVM, MLR, and ANN in predicting nitrogen content in rice using spectral features. These conclusions are consistent with previous prediction studies of other crop traits[80]. The RF model, which is a popular ensemble learning algorithm, utilizes bootstrap resampling to extract multiple sample sets from the original sample, forming sample subsets. Subsequently, independent decision trees are constructed using each sample subset, and the prediction results from multiple decision trees are then fused together[81]. This approach enhances the effectiveness of the RF in dealing with outliers or noise and mitigates the problem of overfitting. Previous studies have demonstrated that the RF model exhibits stability and robustness in dealing with large amounts of data and tends to yield high accuracy[44,82].

Based on the correlation analysis between multiple variables and LAI and SPAD, it was found that there were significant multicollinearity issues among the variables. To address this issue, methods such as PCA, ST, and ST_PCA were employed to reduce the dimensionality of the data[83,84]. The results showed that compared to models without dimensionality reduction, the accuracy of PCA combined with regression models significantly improved, demonstrated by larger R^2 values and smaller RMSE. The PCA method transforms multiple input variables into several independent components to explain the variance of the entire prediction space. In contrast to the PCA approach, ST-VIs and ST-TEs did not enhance the accuracy of model estimation. The ST method essentially identifies the most correlated features among the multivariate variables for modeling. Additionally, the ST_PCA method was further employed to enhance the model's accuracy, where ST_PCA-VIs+TEs combined with RF exhibited the best performance, with R^2=0.86, RMSE=0.26, and MAE=0.22 for LAI estimation, and R^2=0.91, RMSE=2.01, and MAE=1.66 for SPAD estimation (Figure 10). This indicated that when dealing with high-dimensional data and constructing complex prediction models, the stepwise selection in combination with principal component analysis is highly effective. The ST_PCA method has the following advantages: 1) effectively resolved the multicollinearity problem while removing the feature variables with low correlation in the model; 2) reduced overfitting in high-dimensional data; stepwise regression could select the most relevant features, and PCA reduced the dimensionality, which made the model more focused on the important information; 3) improved model interpretability and generalization. The complexity of model computation is reduced, which enhances the efficiency of model training and estimation and enables it to better handle new data.

5 Conclusions

This study evaluated the impact of combining RGB spectral indices and texture features with different modeling methods and data dimensionality reduction methods on the accuracy of estimating corn LAI and SPAD. We developed three linear regression models (multiple linear regression, ridge regression, and partial least squares) and three machine learning algorithms (BP neural networks, random forests, and support vector machines) to estimate LAI and SPAD of winter wheat using 15 vegetation indices and 24 texture features selected. ST, PCA, and ST_PCA were used to eliminate unnecessary remote sensing information to reduce the number of interpretable variables and the complexity of the model. The results indicated that models established using optical vegetation indices had higher accuracy in estimating LAI and SPAD of winter wheat at multiple growth stages compared to models based on texture features. However, the models tended to underestimate large LAI and SPAD values. The combination of optical vegetation indices and texture features significantly improved the estimation accuracy of LAI and SPAD in winter wheat, and the texture features effectively avoided such underestimation. Furthermore, the estimation accuracy of the machine learning models was usually superior to that of the linear regression models, in which RF achieved the best estimates at different growth stages (R^2=0.79, RMSE=0.34, MAE=0.28 for LAI estimated; R^2=0.83, RMSE=2.27, MAE=1.96 for SPAD estimated). In terms of data downscaling, the PCA method excelled for a relatively small number of feature variables (15 and 24). However, the ST_PCA method performed best for a larger number of feature variables. The ST_PCA combined with the RF model achieves the best estimation (R^2=0.86, RMSE=0.26, MAE=0.22 for LAI estimated; R^2=0.91, RMSE=2.01, MAE=1.66 for SPAD estimated) with VIs + TEs as input set.

Acknowledgements

This research was funded by the National Natural Science Foundation of China (Grant No. 52079113 and U2243235) and Sub-project of National Key R&D Program (Grant No. 2022YFD1900402-01).

[References]

[1] Nasrallah A, Baghdadi N, El Hajj M, Darwish T, Belhouchette H, Faour G, et al. Sentinel-1 data for winter wheat phenology monitoring and mapping. Remote Sensing, 2019; 11(19): 2228.

[2] Qiu B W, Luo Y H, Tang Z H, Chen C C, Lu D F, Huang H Y, et al. Winter wheat mapping combining variations before and after estimated heading dates. ISPRS Journal of Photogrammetry and Remote Sensing, 2017; 123: 35–46.

[3] Zhong L H, Hu L N, Zhou H, Tao X. Deep learning based winter wheat mapping using statistical data as ground references in Kansas and northern Texas, US. Remote Sensing of Environment, 2019; 233: 111411.

[4] Li Z H, Jin X L, Wang J H, Yang G J, Nie C W, Xu X G, et al. Estimating winter wheat (Triticum aestivum) LAI and leaf chlorophyll content from canopy reflectance data by integrating agronomic prior knowledge with the PROSAIL model. International Journal of Remote Sensing, 2015; 36(10): 2634–2653.

[5] Verger A, Vigneau N, Chéron C, Gilliot J, Comar A, Baret F. Green area index from an unmanned aerial system over wheat and rapeseed crops. Remote Sensing of Environment, 2014; 152: 654–664.

[6] Darvishzadeh R, Skidmore A, Schlerf M, Atzberger C. Inversion of a radiative transfer model for estimating vegetation LAI and chlorophyll in a heterogeneous grassland. Remote Sensing of Environment, 2008; 112(5): 2592–2604.

[7] Yang G J, Liu J G, Zhao C J, Li Z H, Huang Y B, Yu H Y, et al. Unmanned aerial vehicle remote sensing for field-based crop phenotyping: current status and perspectives. Frontiers in Plant Science, 2017; 8: 1111.

[8] Luo H X, Dai S P, Li M F, Liu E P, Zheng Q, Hu Y Y, et al. Comparison of machine learning algorithms for mapping mango plantations based on Gaofen-1 imagery. Journal of Integrative Agriculture, 2020; 19(11): 2815–2828.

[9] Lan Y B, Huang Z X, Deng X L, Zhu Z H, Huang H S, Zheng Z, et al. Comparison of machine learning methods for citrus greening detection on UAV multispectral images. Computers and Electronics in Agriculture, 2020; 171: 105234.

[10] Yan G J, Hu R H, Luo J H, Weiss M, Jiang H L, Mu X H, et al. Review of indirect optical measurements of leaf area index: Recent advances, challenges, and perspectives. Agricultural and Forest Meteorology, 2019; 265: 390–411.

[11] Gong Y, Yang K L, Lin Z H, Fang S H, Wu X T, Zhu R S, et al. Remote estimation of leaf area index (LAI) with unmanned aerial vehicle (UAV) imaging for different rice cultivars throughout the entire growing season. Plant Methods, 2021; 17: 88.

[12] Yang N, Zhang Z T, Ding B B, Wang T Y, Zhang J R, Liu C, et al. Evaluation of winter-wheat water stress with UAV-based multispectral data and ensemble learning method. Plant and Soil, 2023; 497: 647–668.

[13] Liang L, Di L P, Zhang L P, Deng M X, Qin Z H, Zhao S H, et al. Estimation of crop LAI using hyperspectral vegetation indices and a hybrid inversion method. Remote Sensing of Environment, 2015; 165: 123–134.

[14] Roth L, Streit B. Predicting cover crop biomass by lightweight UAS-based RGB and NIR photography: an applied photogrammetric approach. Precision Agriculture, 2018; 19(1): 93–114.

[15] Wu S, Deng L, Guo L J, Wu Y J. Wheat leaf area index prediction using data fusion based on high-resolution unmanned aerial vehicle imagery. Plant Methods, 2022; 18(1): 68.

[16] Borhan M S, Panigrahi S, Lorenzen J H, Gu H. Multispectral and color imaging techniques for nitrate and chlorophyll determination of potato leaves in a controlled environment. Transactions of the ASABE, 2004; 47(2): 599–608.

[17] Daughtry C S T, Walthall C L, Kim M S, Colstoun E B, Mcmurtrey J E. Estimating corn leaf chlorophyll concentration from leaf and canopy reflectance. Remote Sensing of Environment, 2000; 74(2): 229–239.

[18] Jena B. The effect of phytoplankton pigment composition and packaging on the retrieval of chlorophyll-a concentration from satellite observations in the Southern Ocean. International Journal of Remote Sensing, 2017; 38(13): 1–22.

[19] Eckert S. Improved forest biomass and carbon estimations using texture measures from worldview-2 satellite data. Remote Sensing, 2012; 4(4): 810–829.

[20] Liu Y N, Liu S S, Li J, Guo X Y, Wang S Q, Lu J W. Estimating biomass of winter oilseed rape using vegetation indices and texture metrics derived from UAV multispectral images. Computers and Electronics in Agriculture, 2019; 166: 105026.

[21] Roth L, Aasen H, Walter A, Liebisch F. Extracting leaf area index using viewing geometry effects—A new perspective on high-resolution unmanned aerial system photography. ISPRS Journal of Photogrammetry and Remote Sensing, 2018; 141: 161–175.

[22] Atzberger C, Richter K. Spatially constrained inversion of radiative transfer models for improved LAI mapping from future Sentinel-2 imagery. Remote Sensing of Environment, 2012; 120: 208–218.

[23] Qiao K, Zhu W Q, Xie Z Y, Li P X. Estimating the seasonal dynamics of the leaf area index using piecewise LAI-VI relationships based on phenophases. Remote Sensing, 2019; 11(6): 689.

[24] Zhou X, Zheng H B, Xu X Q, He J Y, Ge X K, Yao X, et al. Predicting grain yield in rice using multi-temporal vegetation indices from UAV-based multispectral and digital imagery. ISPRS Journal of Photogrammetry and Remote Sensing, 2017; 130: 246–255.

[25] Atzberger C, Darvishzadeh R, Immitzer M, Schlerf M, Skidmore A, Maire G. Comparative analysis of different retrieval methods for mapping grassland leaf area index using airborne imaging spectroscopy. International Journal of Applied Earth Observation and Geoinformation, 2015; 43: 19–31.

[26] Jay S, Gorretta N, Morel J, Maupas F, Bendoula R, Rabatel G, et al. Estimating leaf chlorophyll content in sugar beet canopies using millimeter-to centimeter-scale reflectance imagery. Remote Sensing of Environment, 2017; 198: 173–186.

[27] Sun Q, Gu X H, Chen L P, Xu X B, Wei Z H, Pan Y C, et al. Monitoring maize canopy chlorophyll density under lodging stress based on UAV hyperspectral imagery. Computers and Electronics in Agriculture, 2022; 193: 106671.

[28] Viña A, Gitelson A A, Nguy-Robertson A L, Peng Y. Comparison of different vegetation indices for the remote assessment of green leaf area index of crops. Remote Sensing of Environment, 2011; 115(12):

3468–3478.

[29] Zhang X, Sun H, Qiao X X, Yan X B, Feng M C, Xiao L J, et al. Hyperspectral estimation of canopy chlorophyll of winter wheat by using the optimized vegetation indices. Computers and Electronics in Agriculture, 2022; 193: 106654.

[30] Rouse J W, Haas R H, Schell J A, Deering D W. Monitoring vegetation systems in the great plains with ERTS. In: Fraden S C, Marcanti E P, Becker M A, NASA SP-351. Third ERTS-1 Symposium. Washington, DC: Scientific and Technical Information Office, National Aeronautics and Space Administration. 1974; pp.309–317.

[31] Gitelson A A. Wide dynamic range vegetation index for remote quantification of biophysical characteristics of vegetation. Journal of Plant Physiology, 2004; 161(2): 165–173.

[32] Borhan M S, Panigrahi S, Satter M A, Gu H. Evaluation of computer imaging technique for predicting the SPAD readings in potato leaves. Information Processing in Agriculture, 2017; 4(4): 275–282.

[33] Jay S, Baret F, Dutartre D, Malatesta G, Héno S, Comar A, et al. Exploiting the centimeter resolution of UAV multispectral imagery to improve remote-sensing estimates of canopy structure and biochemistry in sugar beet crops. Remote Sensing of Environment, 2019; 231: 110898.

[34] Blancon J, Dutartre D, Tixier M H, Weiss M, Comar A, Praud S, et al. A high-throughput model-assisted method for phenotyping maize green leaf area index dynamics using unmanned aerial vehicle imagery. Frontiers in Plant Science, 2019; 10: 685.

[35] Lu D S. The potential and challenge of remote sensing - based biomass estimation. International Journal of Remote Sensing, 2006; 27(7): 1297–1328.

[36] Yue J B, Yang G J, Tian Q J, Feng H K, Xu K J, Zhou C Q. Estimate of winter-wheat above-ground biomass based on UAV ultrahigh-ground-resolution image textures and vegetation indices. ISPRS Journal of Photogrammetry and Remote Sensing, 2019; 150: 226–244.

[37] Wulder M A, LeDrew E F, Franklin S E, Lavigne M B. Aerial image texture information in the estimation of northern deciduous and mixed wood forest leaf area index (LAI). Remote Sensing of Environment, 1998; 64(1): 64–76.

[38] Hlatshwayo S T, Mutanga O, Lottering R T, Kiala Z, Ismail R. Mapping forest aboveground biomass in the reforested Buffelsdraai landfill site using texture combinations computed from SPOT-6 pan-sharpened imagery. International Journal of Applied Earth Observation and Geoinformation, 2018; 74(9): 65–77.

[39] Yang K L, Gong Y, Fang S H, Duan B, Yuan N G, Peng Y, et al. Combining spectral and texture features of UAV images for the remote estimation of rice LAI throughout the entire growing season. Remote Sensing, 2021; 13(15): 3001.

[40] Zhang J Y, Qiu X L, Wu Y T, Zhu Y, Cao Q, Liu X J, et al. Combining texture, color, and vegetation indices from fixed-wing UAS imagery to estimate wheat growth parameters using multivariate regression methods. Computers and Electronics in Agriculture, 2021; 185: 106138.

[41] Rischbeck P, Elsayed S, Mistele B, Barmeier G, Heil K, Schmidhalter U. Data fusion of spectral, thermal and canopy height parameters for improved yield prediction of drought stressed spring barley. European Journal of Agronomy, 2016; 78: 44–59.

[42] Ma Y R, Ma L L, Zhang Q, Huang C P, Yi X, Chen X Y, et al. Cotton yield estimation based on vegetation indices and texture features derived from RGB image. Frontiers in Plant Science, 2022; 13: 925986.

[43] Jiang J, Johansen K, Stanschewski C S, Wellman G, Mousa M A A, Fiene G M, et al. Phenotyping a diversity panel of quinoa using UAV-retrieved leaf area index, SPAD-based chlorophyll and a random forest approach. Precision Agriculture, 2022; 23(3): 961–983.

[44] Wang L A, Zhou X D, Zhu X K, Dong Z D, Guo W S. Estimation of biomass in wheat using random forest regression algorithm and remote sensing data. The Crop Journal, 2016; 4(3): 212–219.

[45] Li R, Wang D L, Zhu B, Liu T, Sun C M, Zhang Z J. Estimation of nitrogen content in wheat using indices derived from RGB and thermal infrared imaging. Field Crops Research, 2022; 289: 108735.

[46] Inoue Y, Sakaiya E, Wang C. Capability of C-band backscattering coefficients from high-resolution satellite SAR sensors to assess biophysical variables in paddy rice. Remote Sensing of Environment, 2014; 140: 257–266.

[47] Maimaitijiang M, Sagan V, Sidike P, Daloye A M, Erkbol H, Fritschi F B. Crop monitoring using satellite/UAV data fusion and machine learning. Remote Sensing, 2020; 12(9): 1357.

[48] Swatantran A, Dubayah R, Goetz S, Hofton M, Betts M G, Sun M, et al. Mapping migratory bird prevalence using remote sensing data fusion. PLOS One, 2012; 7(1): e28922.

[49] Lopez-Sanchez J M, Ballester-Berman J D, Hajnsek I. First results of rice monitoring practices in Spain by means of time series of terraSAR-X dual-pol images. IEEE Journal of Selected Topics in Applied Earth Observations and Remote Sensing, 2011; 4(2): 412–422.

[50] Wang K, Dickinson R E. Cotton yield estimation using very high-resolution digital images acquired with a low-cost small unmanned aerial vehicle. Transactions of the ASABE, 2016; 59(6): 1563–1574.

[51] Meyer G E, Neto J C. Verification of color vegetation indices for automated crop imaging applications. Computers and Electronics in Agriculture, 2008; 63(2): 282–293.

[52] Gitelson A A, Kaufman Y J, Stark R, Rundquist D. Novel algorithms for remote estimation of vegetation fraction. Remote Sensing of Environment, 2002; 80(1): 76–87.

[53] Bendig J, Yu K, Aasen H, Bolten A, Bennertz S, Broscheit J, et al. Combining UAV-based plant height from crop surface models, visible, and near infrared vegetation indices for biomass monitoring in barley. International Journal of Applied Earth Observation and Geoinformation, 2015; 39: 79–87.

[54] Peñuelas J, Gamon J A, Fredeen A L, Merino J, Field C B. Reflectance indices associated with physiological changes in nitrogen- and water-limited sunflower leaves. Remote Sensing of Environment, 1994; 48(2): 135–146.

[55] Ahmad I S, Reid J F. Evaluation of colour representations for maize images. Journal of Agricultural Engineering Research, 1996; 63(3): 185–195.

[56] Wu J, Wang D, Bauer M E. Assessing broadband vegetation indices and QuickBird data in estimating leaf area index of corn and potato canopies. Field Crops Research, 2007; 102(1): 33–42.

[57] Gamon J A, Surfus J S. Assessing leaf pigment content and activity with a reflectometer. New Phytologist, 1999; 143(1): 105–117.

[58] Sulik J J, Long D S. Spectral considerations for modeling yield of canola. Remote Sensing of Environment, 2016; 184: 161–174.

[59] Verrelst J, Schaepman M E, Koetz B, Kneubühler M. Angular sensitivity analysis of vegetation indices derived from CHRIS/PROBA data. Remote Sensing of Environment, 2008; 112(5): 2341–2353.

[60] Guijarro M, Pajares G, Riomoros I, Herrera P J, Burgos-Artizzu X P, Ribeiro A. Automatic segmentation of relevant textures in agricultural images. Computers and Electronics in Agriculture, 2011; 75(1): 75–83.

[61] Hall-Beyer M. Practical guidelines for choosing GLCM textures to use in landscape classification tasks over a range of moderate spatial scales. International Journal of Remote Sensing, 2017; 38(5): 1312–1338.

[62] Li B, Xu X M, Zhang L, Han J W, Bian C S, Li G C, et al. Above-ground biomass estimation and yield prediction in potato by using UAV-based RGB and hyperspectral imaging. ISPRS Journal of Photogrammetry and Remote Sensing, 2020; 162: 161–172.

[63] Liang Y Y, Kou W L, Lai H Y, Wang J, Wang Q H, Xu W H, et al. Improved estimation of aboveground biomass in rubber plantations by fusing spectral and textural information from UAV-based RGB imagery. Ecological Indicators, 2022; 142: 109286.

[64] Zhang C Y, Xie Z X. Combining object-based texture measures with a neural network for vegetation mapping in the Everglades from hyperspectral imagery. Remote Sensing of Environment, 2012; 124: 310–320.

[65] Williams P C, Norris K H. Near-infrared technology in the agricultural and food industries. American Association of Cereal Chemists, Inc. 1987; pp.293-313.

[66] Wold S, Sjöström M, Eriksson L. PLS-regression: a basic tool of chemometrics. Chemometrics and Intelligent Laboratory Systems, 2001; 58(2): 109–130.

[67] Zhang X W, Zhang K F, Sun Y Q, Zhao Y D, Zhuang H F, Ban W, et al. Combining spectral and texture features of UAS-based multispectral images for maize leaf area index estimation. Remote Sensing, 2022; 14(2): 331.

[68] Li R, Wang D L, Zhu B, Liu T, Sun C M, Zhang Z J. Estimation of grain yield in wheat using source-sink datasets derived from RGB and thermal infrared imaging. Food and Energy Security, 2023; 12(2): e434.

[69] Reddy Maddikunta P K, Hakak S, Alazab M, Bhattacharya S, Gadekallu T R, Khan W Z, et al. Unmanned aerial vehicles in smart agriculture: applications, requirements, and challenges. IEEE Sensors Journal, 2021;

21(16): 17608–17619.
[70] Kong B, Yu H, Du R X, Wang Q. Quantitative estimation of biomass of alpine grasslands using hyperspectral remote sensing. Rangeland Ecology Management, 2019; 72(2): 336–346.
[71] Zhang J Y, Liu X, Liang Y, Cao Q, Tian Y C, Zhu Y, et al. Using a portable active sensor to monitor growth parameters and predict grain yield of winter wheat. Sensors, 2019; 19(5): 1108.
[72] Cao Y F, Xu H L, Song J, Yang Y, Hu X H, Wiyao K T, et al. Applying spectral fractal dimension index to predict the SPAD value of rice leaves under bacterial blight disease stress. Plant Methods, 2022; 18: 67.
[73] Yamaguchi T, Tanaka Y, Imachi Y, Yamashita M, Katsura K. Feasibility of combining deep learning and RGB images obtained by unmanned aerial vehicle for leaf area index estimation in rice. Remote Sensing, 2021; 13(1): 84.
[74] Duan B, Liu Y T, Gong Y, Peng Y, Wu X T, Zhu R S, et al. Remote estimation of rice LAI based on Fourier spectrum texture from UAV image. Plant Methods, 2019; 15: 124.
[75] Guo A T, Huang W J, Dong Y Y, Ye H C, Ma H Q, Liu B, et al. Wheat yellow rust detection using UAV-based hyperspectral technology. Remote Sensing, 2021; 13(1): 123.
[76] Reddersen B, Fricke T, Wachendorf M. A multi-sensor approach for predicting biomass of extensively managed grassland. Computers and Electronics in Agriculture, 2014; 109: 247–260.
[77] Yuan W S, Meng Y, Li Y, Ji Z G, Kong Q M, Gao R, et al. Research on rice leaf area index estimation based on fusion of texture and spectral information. Computers and Electronics in Agriculture, 2023; 211: 108016.
[78] Zhang Y M, Ta N, Guo S, Chen Q, Zhao L C, Li F L, et al. Combining spectral and textural information from UAV RGB images for leaf area index monitoring in kiwifruit orchard. Remote Sensing, 2022; 14(5): 1063.
[79] Zha H N, Miao Y X, Wang T T, Li Y, Zhang J, Sun W C, et al. Improving unmanned aerial vehicle remote sensing-based rice nitrogen nutrition index prediction with machine learning. Remote Sensing, 2020; 12(2): 215.
[80] Lee H, Wang J, Leblon B. Using linear regression, random forests, and support vector machine with unmanned aerial vehicle multispectral images to predict canopy nitrogen weight in corn. Remote Sensing, 2020; 12(13): 2071.
[81] Lin C S, Chen S Y, Chen C C, Tai C H. Detecting newly grown tree leaves from unmanned-aerial-vehicle images using hyperspectral target detection techniques. ISPRS Journal of Photogrammetry and Remote Sensing, 2018; 142: 174–189.
[82] Verrelst J, Rivera J P, Veroustraete F, Muñoz-Marí J, Clevers J G P W, Camps-Valls G, et al. Experimental sentinel-2 LAI estimation using parametric, non-parametric and physical retrieval methods–A comparison. ISPRS Journal of Photogrammetry and Remote Sensing, 2015; 108: 260–272.
[83] Karpouzli E, Malthus T J, Place C J. Hyperspectral discrimination of coral reef benthic communities in the western Caribbean. Coral Reefs, 2004; 23(1): 141–151.
[84] Elmasry G, Sun D, Allen P. Non-destructive determination of water-holding capacity in fresh beef by using NIR hyperspectral imaging. Food Research International, 2020; 44(9): 2624–2633.